INTERNATIONAL JOURNAL OF HYDROGEN ENERGY 46 (2021) 4917–4935

Available online at www.sciencedirect.com

ScienceDirect

journal homepage: www.elsevier.com/locate/he

Methane pyrolysis in a molten gallium bubble column reactor for sustainable hydrogen production: Proof of concept & techno-economic assessment

Brandon José Leal Pérez [a], *José Antonio Medrano Jiménez* [a], *Rajat Bhardwaj* [b], *Earl Goetheer* [b], *Martin van Sint Annaland* [a], *Fausto Gallucci* [a,*]

[a] *Inorganic Membranes and Membrane Reactors, Department of Chemical Engineering and Chemistry, Eindhoven University of Technology, P.O. Box 513, Eindhoven, 5600 MB, the Netherlands*

[b] *TNO, Department of Sustainable Process and Energy Systems, Leeghwaterstraat 44, Delft, 2628 CA, The Netherlands*

HIGHLIGHTS

- Methane pyrolysis has been carried out in molten metal bubble columns.
- A techno economic analysis has been carried out.
- Clean hydrogen is produced at a cost comparable to the one without CO2 capture.
- The economics depend on the quality of carbon formed and type of process integration.

ARTICLE INFO

Article history:
Received 31 August 2020
Received in revised form
6 November 2020
Accepted 8 November 2020
Available online 3 December 2020

Keywords:
Methane pyrolysis
Molten metal
Carbon
Bubble column
Techno-economic assessment
Sensitivity analyses

ABSTRACT

Nowadays, nearly 50% of the hydrogen produced worldwide comes from Steam Methane Reforming (SMR) at an environmental burden of 10.5 $t_{CO2,eq}/t_{H2}$, accelerating the consequences of global warming. One way to produce clean hydrogen is via methane pyrolysis using melts of metals and salts. Compared to SMR, significant less CO_2 is produced due to conversion of methane into hydrogen and carbon, making this route more sustainable to generate hydrogen. Hydrogen is produced with high purity, and solid carbon is segregated and deposited on the molten bath. Carbon may be sold as valuable co-product, making industrial scale promising. In this work, methane pyrolysis was performed in a quartz bubble column using molten gallium as heat transfer agent and catalyst. A maximum conversion of 91% was achieved at 1119 °C and ambient pressure, with a residence time of the bubbles in the liquid of 0.5 s. Based on in-depth analysis of the carbon, it can be characterized as carbon black. Techno-economic and sensitivity analyses of the industrial concept were done for different scenarios. The results showed that, if co-product carbon is saleable and a CO_2 tax of 50 euro per tonne is imposed to the processes, the molten metal technology can be competitive with SMR.

* *Corresponding author.*
E-mail address: f.gallucci@tue.nl (F. Gallucci).
https://doi.org/10.1016/j.ijhydene.2020.11.079

Introduction

On 12th December 2015, 195 countries set the basis of the Paris Agreement. They agreed to keep the mean global temperature increase below 2 °C above pre-industrial levels by 2100. Moreover, they committed to developing technologies that can limit the temperature rise to 1.5 °C. Nevertheless, this limit represents a big challenge when looking at the temperature history over the last 160 years. The global mean temperature from before 1860–2020 has increased approximately 1.4 °C [1,2]. Considering the last 40 years the temperature increase has been nearly 1 °C, which is the highest rate of increase in history [1,2]. During the same period, the global CO_2 concentration has skyrocketed from 340 to 416 ppm, which represents an unprecedented average increase rate of almost 2 ppm/year [2]. The increase of world population implies higher energy demands, which will result in generating more CO_2 with the actual fossil fuel dominated energy mix. The current environmental policies are still far from meeting the goals set in the Paris Agreement. In the past decades, efforts have been made focused on developing sustainable, CO_2-neutral energy sources. One of them is hydrogen, which does not generate CO_2 emissions in its combustion with air (or when used in electrochemical energy systems). Its application as feedstock for fuel cells to power electric cars is promising and increases its demand by the automotive industry. However, 96% of the world's hydrogen production use fossil fuel-based technologies, emitting tremendous amounts of CO_2. Specifically, 48% of these processes use natural gas (NG) as feedstock, 30% use petroleum and 18% use coal. Only 4% of the H_2 is made from renewable sources, such as water electrolysis [3]. The current benchmark process for H_2 production is Steam Methane Reforming (SMR), which consists of the chemical conversion of natural gas with steam to produce carbon monoxide and hydrogen. A subsequent reaction step known as water gas shift (WGS) is carried out in order to improve the production of hydrogen and thus the H_2/CO ratio. A by-product of this reaction is CO_2, and it is produced at the same rate as methane is consumed. The produced H_2 is then separated in a Pressure Swing Adsorption unit (PSA) with high purity. In addition, the PSA off-gas is often used as part of the fuel for steam generation, releasing CO_2 after combustion. In fact, SMR emits over 10.5 $t_{CO2,eq}/t_{H2}$ (i.e. 0.48 $mol_{CO2,eq}/mol_{H2}$), which pollutes the environment and increases the negative environmental impact made by mankind [4]. To mitigate this, the scientific community is currently working towards novel technologies for sustainable hydrogen production [3,5–9].

Methane pyrolysis. A CO_2-free sustainable technology

Methane pyrolysis is a relatively simple process to produce high purity hydrogen with the extra advantage that carbon oxides (CO/CO_2) are not produced. This process is moderately endothermic, and yields hydrogen and solid carbon as indicated in Eq. (1) [4].

$$CH_4(g) \Leftrightarrow C(s) + 2H_2(g) \quad \Delta H^0_{net} = 74.8 kJ/mol_{CH_4} \tag{1}$$

Two moles of hydrogen are formed per mol of methane via methane pyrolysis. This ratio is unfavorable compared to SMR, where both steam reforming and water gas shift reactions improve the balance up to four. From a chemical equilibrium perspective, and following Le Châtelier's principle, low pressures and high temperatures drive the reaction towards the products. The effect of temperature and pressure on the equilibrium conversion of methane is presented in Fig. 1 for a range of pressures from 1 to 35 bar and temperatures from 100 to 1500 °C.

As seen in Fig. 1, the equilibrium-limited reaction may require temperatures over 900 °C at 1 bar in order to achieve conversions over 95%. It has been reported that conversions over 90% have been achieved at short residence times (<1.5 s) within the temperature range 1450–1500 °C [11]. Pyrolysis of methane at these conditions is however very energy-intensive, and therefore solid, metal-based catalysts have been further developed to decrease the reaction temperature. Unfortunately, it was proven that by using nickel-based catalysts, carbon nanofibers are deposited on the active phase of the catalyst, leading to rapid deactivation. Researchers have carried out several analysis from an energetic and economic point of view to evaluate the possibility of using carbon as catalyst [12]. In fact, the authors demonstrated that methane pyrolysis was possible under SMR common temperatures (i.e. 800-900 °C), by using disordered carbon materials with high surface areas. They concluded that the catalytic properties of carbons were mainly determined by their structural and surface properties, which means that the surface concentration of high-energy sites constituted the key factor of their activity [13]. Moreover, several studies using char coal, activated carbon or carbon black as catalysts were performed [14]. The conclusion was that activated carbon performed best, followed by carbon black, however catalyst deactivation occurred in all cases due to the high amounts of carbon formed over time. Therefore, further developments are still needed to ensure a constant activity of catalysts to perform methane pyrolysis at low temperatures.

The co-produced carbon is a valuable material with many applications in industry, depending on its quality. Most common forms of carbon are petroleum coke, carbon black, activated carbon, and carbon filaments. Carbonaceous materials are used as adsorbents, catalyst and catalyst supports (activated carbon); as structural and tensile-force resisting materials (carbon filaments) and in the rubber tire industry (carbon black) [12,15,16]. The selling prices vary sensitively from type of carbon. For coke and carbon black, prices range 150–400 €/t and 500–1000 €/t, respectively, whereas for activated carbon the prices can be up to 1500–1800 €/t and even 1 M€/t for carbon filaments [12,17]. At industrial scale it is important to characterize the produced carbon, given that its quality has an impact on the total revenues and process economics, providing that all the produced carbon in the plant has its market.

According to the International Energy Agency's Global Trends and Outlook for Hydrogen Report [18], global hydrogen market is estimated to value 154.74 billion $ in 2022. The global demand of pure hydrogen in 2018 was almost 74 Mtonnes, and recent trends show an increase in demand of approximately 2 Mtonnes/year [19], reaching over 80 Mtonnes in 2022. Considering that 48% of the world's hydrogen production is made by SMR, more than 38 $Mtonnes_{H2}$/year would be

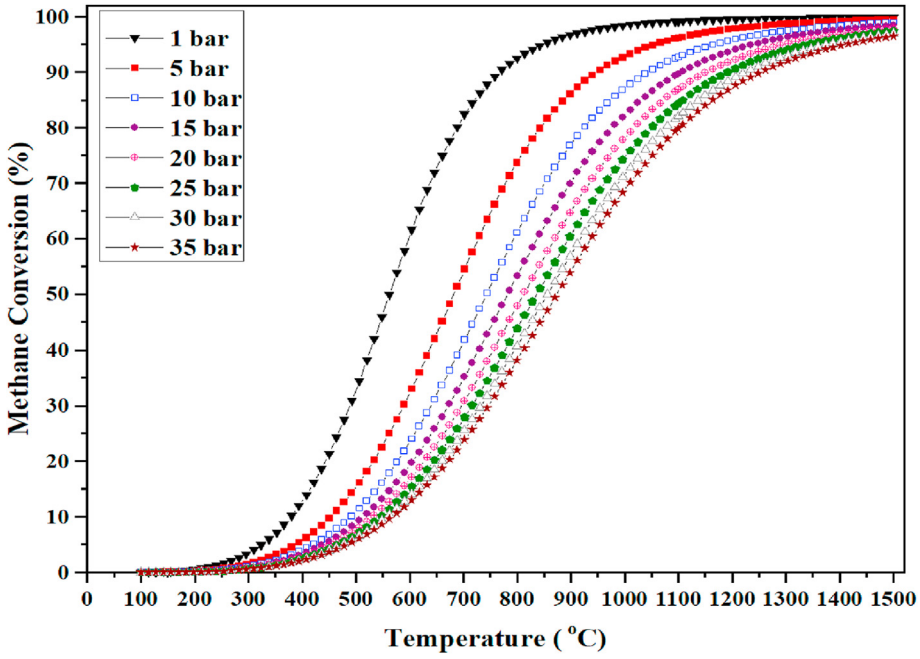

Fig. 1 – Equilibrium conversion of methane with temperature and pressure in Aspen Plus® v10. Based on [10].

produced and almost 400 $Mtonnes_{CO2}$/year would be emitted. In order to make a difference in the reduction of CO_2 emissions, similar hydrogen throughput should be produced by methane pyrolysis technology. However, to reach such amount per year more than 100 Mtonnes of carbon would be produced, and the annual worldwide carbon market is around 13.6–18 Mtonnes [12]. This means that the carbon market should increase 6–8 times for a viable exit of the carbon, constituting the main constraint for industrial implementation. That is why methane pyrolysis has been labeled as "bridge technology" from fossil fuels to greener and more sustainable processes, and medium-scale plants should be considered first in order to assess its feasibility [20]. Another interesting approach to propose a sustainable exit of the carbon surplus, in order to increase the global production of hydrogen by methane pyrolysis, focuses on the storage of solid carbon as a back-up energy source for the future, when CO_2 capture technologies are fully developed.

Methane pyrolysis using melts: molten metals and salts

The first-known manuscript wherein the use of molten metals (MMs) was proposed for hydrogen production is an US Patent in 1931 by Daniel Tyrer [21]. He proposed the use of molten iron to dissolve carbon and to burn the mixture jointly with air in a different chamber. This enabled sufficient heat for the process and for keeping the iron molten. In recent decades, the use of MMs for methane pyrolysis has been widely investigated. For instance, Steinberg [22] proposed in 1999 a reactor concept which consisted of a molten metal bath of tin/copper, in order to promote the heat transfer from the bath to the upcoming methane (upwards) in a bubbling reactor configuration. He pointed out its benefits in terms of carbon separation, which would be placed on top of the molten metal bath, but also in terms of heat transfer enhancement. Moreover, Wang et al. [23] proposed molten magnesium as the liquid media for the thermal decomposition of methane. They found out that the energy required to form 1 mol of hydrogen was 65.1% the energy needed for SMR. However, the stability of magnesium at high temperatures was proven very low due to vaporization of the metal, limiting its scale-up.

MMs possess unique properties as heat transfer media, avoiding temperature losses or ramps along the reactor's height. Besides, MMs have been widely used in steel industry and metallurgy, therefore it does not represent a technical challenge for the field. Phase segregation of hydrogen and carbon may be reached based on density difference, as carbon is lighter than any of the above-mentioned metals. Moreover, carbon's low volatility and solubility in liquids allow its deposition on top of the molten media, facilitating its separation and handling. Carbon can be easily removed in a continuous process using floatation cell technology, which is normally performed in slag removal [24]. In blast furnaces, a set of pipes is employed to tap both slag and molten iron from different heights of the furnace [25].

MMs, when mixed with metallic elements or alloys, may also present catalytic properties. For instance, a work recently done by Esrafilzadeh et al. [26] reported that CO_2 can be reduced to solid carbon at room temperature using a cerium-containing liquid galinstan as electrocatalyst. Recently, Upham et al. [27] provided a comparison of the catalytic activity of different molten media for methane pyrolysis, and it was reported that a liquid catalyst composed of 17% Ni – 83% Bi had the highest rate of hydrogen production, with a value of $9.0 \cdot 10^{-8}$ mol H_2 prod./cm^2.s. However, a liquid catalyst with 27% Ni – 73% Bi achieved the highest methane conversion of methane (95%) at 1065 °C. Ni is the active phase for cracking, which is not deactivated by coking as the gas passes through the melt and drags the produced carbon to the top of the liquid metal surface, thus achieving high performance.

Currently, molten salts have also been investigated as catalysts for methane pyrolysis. A CH_4 conversion of approximately 55% and H_2 selectivity of 99% were reported using a molten mixture of 67% $MnCl_2$–KCl 33% in a continuous run of 30 h at 1050 °C [28]. A more modest CH_4 conversion of 9% at 1000 °C was achieved by a Fe (3%)-NaKCl molten mixture after 50 h of continuous run, showing no signs of deactivation [29]. The use of molten salts as an intermediate layer between the MMs and solid carbon has been also investigated for carbon purification. Recently, several authors, Rahimi et al. [30] reported that the addition of molten bromide salts in a reactor containing a liquid catalyst with 27% Ni – 73% Bi reduced the metal impurities of the produced carbon to less than 0.1 wt%.

Reactor design for the technology: the liquid metal bubble column reactor

Many efforts have been focused on the design of the liquid metal bubble column reactor (LMBCR), which works at high temperatures (750–1200 °C) and atmospheric pressure. The most employed MM has been tin [31–34]. Tin is a highly stable metal, with vapor pressures as low as 1.1 Pa at 1300 K. Its shrinkage on solidification (2.8%) ensures good mechanical strength of the construction materials for the reactor, such as quartz or stainless steel (SS), and it reduces its volume by cooling after operation [35]. Table 1 summarizes the scientific efforts regarding the development of a LMBCR using molten tin.

In Table 1, parameters such as the residence time of the gas in the liquid (τ_L) or type of bubbles generator are presented, and these parameters play a significant role in the reaction performance. Values of the τ_L were calculated by Serban et al. [10] using the approach for gas bubble velocity determination under laminar flow conditions in molten metals, previously reported by Andreini et al. [36]. The use of SS reactors for high-temperature operations (>900 °C) is not recommended due to the strong corrosion effects of molten tin on the steel [34,37]. In contrast, quartz is corrosion-resistant and mechanically stable at harsh conditions, making it a suitable reactor material [33]. Furthermore, tin improves heat transfer from the energy source to the bubbles. For a constant inlet gas flow higher liquid metal volumes are desired in the system because τ_L is increased. However, the highest methane conversion value (51%) was achieved with the lowest reaction temperature and τ_L of the three reactors. This suggests that other factors may play a role in the pyrolysis, such as the bubbles generator. By using porous distributors, the production of small bubbles along the reactor's diameter improves the conversion of methane. Small bubbles allow higher gas-liquid interfacial areas for the cracking reaction, even at relatively low cracking temperatures (750 °C). The use of a porous plate distributor seems to be optimal compared to the single orifices proposed by Plevan et al. [32] and Geißler et al. [33]. In fact, the lowest methane conversion was achieved with the highest diameter of the orifice (1 mm), even though τ_L is approximately 5 times higher than that for the reactor with porous distributor. This means that the use of an orifice does not effectively disperse the bubbles along the reactor, and these bubbles are bigger than that of porous distributors, implying lower gas-liquid interfacial areas which limit conversion. With a reduction of 50% in the orifice size (i.e. 0.5 mm), and the highest τ_L and temperature among the three studies, the conversion improved up to 32%. Nevertheless, this performance was not as efficient as the one reported by Serban et al. [10]. The use of a porous plate distributor, high temperatures and high τ_L are considered to be key parameters to enhance reactor performance. An innovative configuration of the LMBCR was proposed in 2016 by Geißler et al. [34], reporting high hydrogen throughput. In this research, a highly porous packed bed made of cylindrical quartz rings is embedded inside quartz tube, filled with molten tin. The quartz tube is protected by a SS tube of 1150 mm length and 49.25 mm inner diameter. The introduction of the packed bed enabled better control and homogeneity of the residence time, as the residence time decreases from the bottom to the top because bubble size increases due to the molar expansion by formation of hydrogen. The maximum hydrogen yield (78%) was found at 1175 °C and 50 mL_n/min, with less than 2 mol% of intermediate products (ethylene, ethane). Despite extensive research, many aspects on how the reaction takes place remain unclear. In this work, a LMBCR using pure gallium and a quartz porous plate for bubbles distribution was designed and tested for methane pyrolysis. Gallium was chosen due to its low melting point (29.7 °C), viscosity (0.59 cP at 1010 °C), and easy handling [38,39]. Upham et al. [27] also reported that gallium may present catalytic properties in pyrolyzing methane, with a hydrogen production rate of $3.2 \cdot 10^{-9}$ mol H_2 prod./cm^2.s, although this productivity is on average one order of magnitude lower than that of a Bi–Ni combination, as mentioned earlier. The main objective was the demonstration of the concept by using a quartz-based reactor in a bubble column configuration with a quartz porous plate, and pure gallium as the molten metal. No reactor with these characteristics was tested before in literature. Conversion measurements were done with the presence of molten gallium but also in empty reactors, to set a reference case. The experiments with gallium were done to assess whether the liquid media acts as a catalyst or simply as a heat transfer media for the reaction. Furthermore, the influence of τ_L on both methane conversion and carbon segregation was evaluated. The quality of the generated carbon was characterized to assess its market value. Finally, different plant configurations were proposed for the concept at industrial scale. Thermodynamic, techno-economic and sensitivity analyses were

Table 1 – The LMBCR properties, operating conditions and performance. Adapted from [34].

Source	Reactor Material	Bubbles Generator	MM	τ_L (s)	Temp. (°C)	CH_4 conversion (%)
Serban et al. [10]	SS	MOTT® 0.5 μm porous distributor	Tin	0.5–0.3	750	51
Plevan et al. [32]	SS	1 mm orifice	Tin	2.7–1.7	900	18
Geißler et al. [33]	Quartz	0.5 mm orifice	Tin	4.9–3.2	1000	32

made for comparison of the proposed configurations with the benchmark technology (SMR).

Materials and methods

Reactor

The reactor concept is depicted in Fig. 2.

In Fig. 2, it is observed that pure methane is fed at the bottom of the reactor, which has inside a molten metal bath on top of a porous plate, which homogeneously distributes the gas phase along the reactor, and where bubbles are formed by the contact between the uprising gas and the liquid media. At that point, the reaction in Eq. (1) would take place at the gas-liquid interface between the bubble and molten gallium. The bubble would increase its size due to the increase in volumetric gas flow by molar expansion, caused by production of hydrogen. In fact, the volumetric gas flow would double the initial gas flow upon 100% conversion of methane is achieved. In principle, the bubble diameter is estimated to be 1.26 times the initial size, value which comes from the ratio between final (100% H_2) and initial (100% CH_4) bubble volumes. In practice, bigger bubbles may be formed by coalescence. The hydrostatic pressure head caused by the heavy molten metal may play a role in bubble size distribution, although its effect decreases along the height of the liquid. Carbon would then be generated and deposited homogeneously along the interface, and the reaction would finish once the entire interface is covered by carbon. The bubbles would continue their ascension until they reach the molten gallium surface. In here, the bubbles would pop, releasing both hydrogen and carbon, the latter being deposited in layers on top of the molten metal bath due to differences in density, achieving full segregation of phases. Hydrogen subsequently leaves the reactor at the outlet and flows downstream the process.

Materials and experimental set-up

The material used in this work was gallium with a minimum purity of 99.99%, supplied by Rotometals. The reactor consists of a U-shaped vessel of 3 mm thick quartz tube equipped with a DURAN® quartz porous plate of 36 mm in diameter, with the biggest nominal pore size distribution available (160–250 μm), in order to reduce the pressure drop in the system. The reactor is placed inside a 360 mm height electrical oven (ELICRA Split Furnace). The reaction volume is approximately 350 mL. The experimental apparatus is presented in Fig. 3.

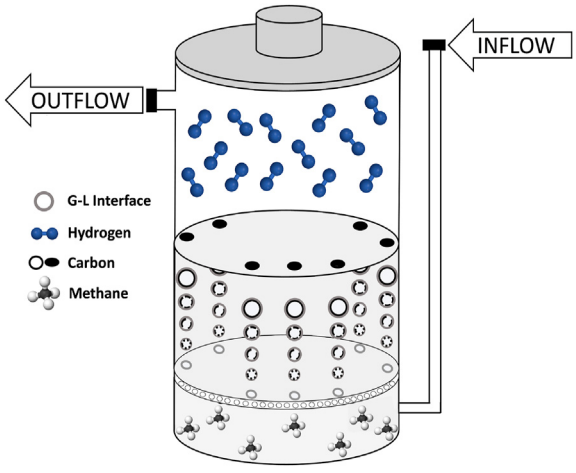

Fig. 2 – Methane cracking reaction inside a LMBCR using pure gallium and a quartz bubbles distributor.

The reactor is embedded in an electrical oven with 3 independent heating zones, all of them equipped with their own temperature controllers and sensors, TC's 1–3 and TE's 1–3 respectively. The inner electrical resistances and ceramic isolation enable reaction temperatures as high as 1150 °C. For a more accurate monitoring of the temperature profile along the reactor, 3 notches of 2 mm, evenly spaced by 160 mm, were created at the reactor's outer wall to assemble 3 thermocouples (TE's 4–6). Argon, nitrogen, methane, hydrogen and air were available in the setup and controlled by 3 Bronkhorst mass flow controllers (MFC's 1–3). Relief valves were placed in the gas lines to ensure process safety (SV's 1–5), as well as check valves (CV's 1–3), to avoid back-flow of gas. The gases were fed at atmospheric pressure, monitored by the pressure transducer PT-1, and were subsequently preheated before reaching the porous plate distributor. The outlet gas leaves the reactor at nearly ambient conditions, registered by the pressure transducer PT-2 and the thermocouple TE-7. For gas chromatography, a slight pressure difference of around 0.3 bar was required for its correct use. The change in pressure was achieved by using a manually actioned needle valve (NV), placed before a digital pressure indicator (PI). The gases were finally sent to the exhaust. The experiments were driven towards the validation of the concept, using a diluted feed mixture consisting of 50-50% Ar-CH_4 at a standard volumetric flow of 450 mL/min. By using a diluted mixture, the partial pressure of methane inside the reactor is reduced and the equilibrium shifts to the right, according to Le Châtelier's principle for gas-phase reactions at constant reactor pressure. This flow rate in empty reactors enabled a minimum gas residence time of 46 s at ambient conditions and, after volumetric expansion of the gas by increase in temperature, a minimum of 10 s was estimated for the highest temperature (1100 °C). The temperature registered by sensor TE-5 was chosen to indicate the reaction temperature, given its position in the middle of the heating zones. Two sets of experiments were carried out in this work. Firstly, thermal cracking of methane was performed in the reactor without any molten gallium (will be hereafter referred to as blank experiments). These experiments mainly focused on achieving methane conversions at different cracking temperatures and also on the identification of reaction intermediates, which could also be formed in the reaction. These blank experiments did not only set a baseline for comparison with the experiments including the molten metal, but also allowed the collection of the obtained carbon for characterization. On the other hand, experiments with increasing quantity of molten gallium were done in order to determine its effect on methane pyrolysis. Liquid gallium was filled in the reactor until reaching a liquid height of 50 mm and 150 mm for methane pyrolysis. This implied a volumetric fraction of liquid inside the reactor of 14% and 43%, respectively.

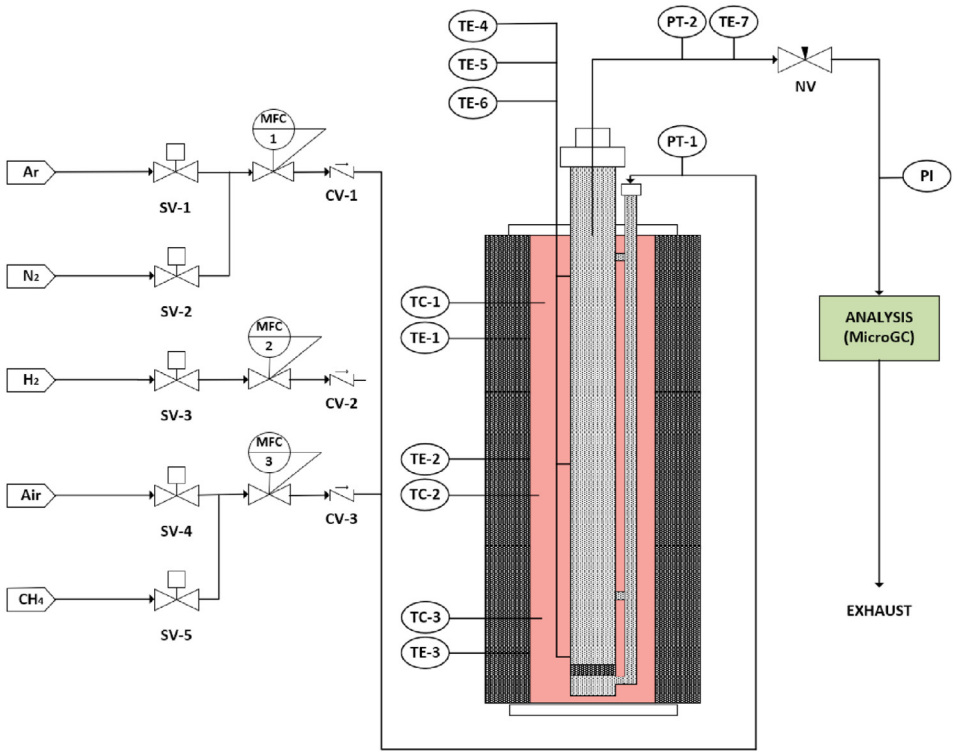

Fig. 3 – Experimental apparatus for the thermal cracking of methane using molten gallium.

Characterization techniques

Gas chromatography

The outlet gases from the reactor were analyzed by a 490 Micro GC, provided by Agilent Technologies. The Micro GC consisted of two modules with two different columns for molecular sieving. The first column was a molecular sieve of 5 Å, which utilized Helium as carrier gas and detected gases such as argon, methane and carbon dioxide. The second one was a CO_x column that used argon as carrier gas and detected helium, hydrogen and air. An external standard method was performed to determine the concentrations of the gases in the mixture.

Raman spectroscopy

Raman spectroscopy was used to determine the structure of the carbon samples for quality assessment. The technique consisted of injecting a laser beam of a specific wavelength to bring the C–C bonds to an excitation state, which allowed the measurement in the form of spectra. The carbon samples were tested in a WITec Alpha 300 Raman Spectrometer using a laser beam with an intensity of 633 nm.

Brunauer–Emmett–Teller (BET) surface area

The determination of the BET surface area and the average pore size was necessary to characterize the carbon samples. A Micromeritics Tristar 3020 Analyzer was used for such purpose. The analysis was performed in two steps: degassing method for cleanup and surface area analyzer. A degassing cleaning method for 6 h, in inert atmosphere with N_2 at 300 °C and vacuum pressure was carried out before each analysis. Following this procedure, BET surface areas and average pore sizes were obtained for 3 carbon samples, produced at average temperatures of 950, 1000 and 1030 °C. They were tested in order to evaluate the effect of temperature on the carbon properties.

Description of the industrial concept

The industrial concept using molten gallium is proposed in this work. Here, natural gas (NG) replaces pure methane as the desired feedstock due to its abundance for industrial processes. Medium-size plants for a hydrogen capacity of 0.75 kg/s or 21 kilotonnes per annum (kta) were simulated using Aspen Plus® v10 according to specific case scenarios, which are described further in the text. The general process scheme consists of a reaction stage, heat integration stages with generation of steam for electricity production; and purification & compression stages for both H_2 and CO_2. This is illustrated in Fig. 4.

In the reaction stage, natural gas is pre-heated and conditioned to the reactor pressure before entering the reactor. The reactor operates at 10 bar, in order to reduce reactor volume and H_2 compression costs, and a temperature of 1200 °C is chosen to compensate the loss of conversion by working at pressures higher than atmospheric. It is assumed that the reaction in Eq. (1) achieves equilibrium at such conditions and at extremely short residence times, mainly due to the high surface areas of microbubbles which are generated by the porous distributor. Pyrolysis with molten gallium allows complete segregation of hydrogen (gas) and carbon (solid). Hydrogen exits the reactor at the

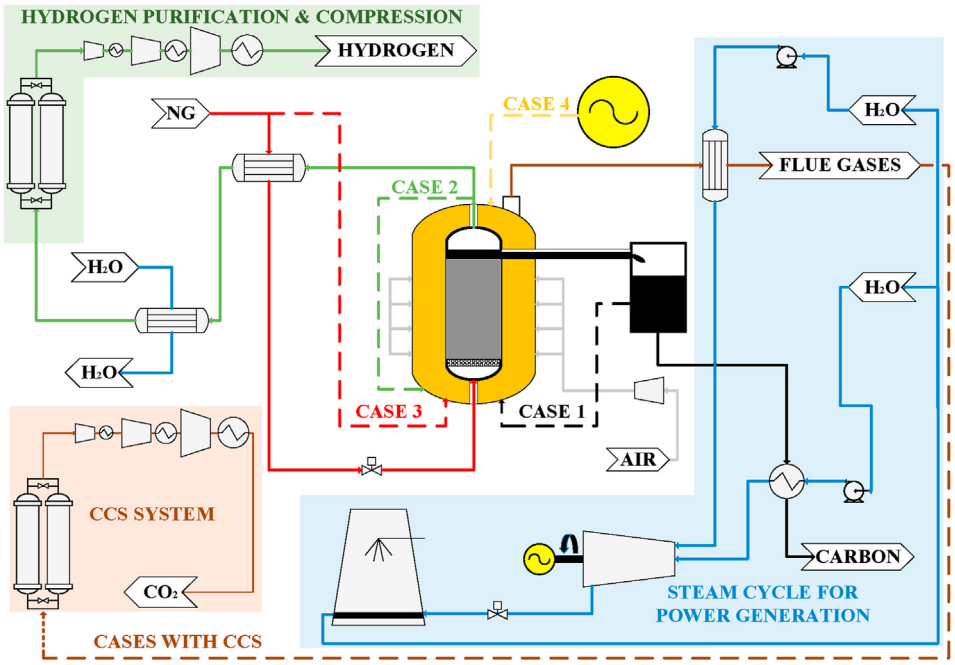

Fig. 4 – The industrial concept. Main process stages and cases scenarios for the energy supply to the reactor.

top, and carbon is deposited on the surface of the molten metal. It exits the reactor by gravity inside a high-temperature resistant pipe and a series of reducing valves, which are placed along the pipe to decrease the pressure up to 1 bar. This practice is similar to the one employed for slag removal in blast furnaces [40,41]. The reactor cannot work at adiabatic conditions since it is an endothermic reaction, and eventually the necessary temperature for the pyrolysis would not be reached. The isothermal operation requires continuous supply of energy, which can be provided by burning fuels or by implementation of an electric arc furnace. In this concept, 4 different cases were considered.

Case 1. It considers the combustion of a fraction of the produced carbon in a burner, to meet the energy demands of the pyrolytic reactor. By burning carbon, the production of H_2 per mol of natural gas reaches its maximum and therefore extra natural gas is not needed for the process. The CO_2 emissions, product of its combustion, represents the main limitations. Considering that CO_2 may be collected in a carbon capture and storage unit (CCS), 2 subcases of Case 1 are studied: Case 1 without CCS (C1) and Case 1 with CCS (C1+CCS).

Case 2 (C2). This case considers combustion of hydrogen inside the burner, generating steam. This alternative is inherently based on the precombustion capture CCS technique. In addition, carbon revenues are maximized because any amount is utilized for energy supply. However, more NG needs to be pyrolyzed in a bigger reactor, in order to meet the hydrogen capacity of the plant, thus increasing the operating and capital costs.

Case 3. This case proposes the use of additional NG as fuel source for the burner, in order to maximize the production and selling of both carbon and H_2. The combustion will also lead to CO_2 emissions. Again, 2 subcases are studied: Case 3 without CCS (C3) and Case 3 with CCS (C3+CCS).

Case 4 (C4). This case considers the use of electricity in an electric arc furnace to supply the necessary energy to the reactor. CO_2 is not produced in this process, but it is assumed that electricity is supplied by a non-renewable conventional source, implying associated CO_2 emissions. The capital cost is reduced due to the lack of a burner, a heat exchanger network to cool down the flue gases after combustion and the absence of CCS technology.

The heat integration stage provides the necessary heat/cooling requirements of the different streams/units of the process. For the hot carbon, moving bed heat exchangers are required for cooling down. A set of shell-and-tube heat exchangers is used to conditioning H_2 and fuel gases prior purification and compression. The purification of H_2 is carried out by a pressure swing adsorption (PSA) unit, and the subsequent compression is achieved by a multi-stage compressor with inter-stage cooling. Electricity for the compressors, pumps or air blower is generated by an intermediate pressure steam turbine. The steam needed for the turbine is generated inside the plant by taking advantage of the extremely hot flue gases stream together with the solid carbon stream. Subsequently, the flue gases stream needs to be further treated in a CCS unit. The chosen CCS technology is a conventional post-combustion carbon capture which uses amines such as monoethanolamine (MEA) for the chemical absorption of CO_2 [42]. Solvent recovery is done in a stripping column using steam, which absorbs the CO_2 from the amine, demanding considerable amounts of energy [43]. The CO_2 is purified by condensation of steam and compressed in a multi-stage compressor with inter-stage cooling.

The selection of construction materials for equipment is crucial in this energy-intensive process. The reactor material is the high-nickel-chromium-iron alloy 602CA® (also known as Nicrofer® 6025HT), which has been reported to withstand operating temperatures above 1200 °C, even in oxidative environments [44–46]. The burner and the electric arc furnace are both considered to be made of carbon steel, lined with a 500-mm layer of MgO–C refractory brick, which can withstand temperatures of even 1500 °C [4,47]. The shell-and-tube heat exchangers are made of SS 316 (shell) and Haynes® 556® alloy (tube). The maximum long-term exposure temperature of these materials are 870 °C [48] and 1095 °C [49], respectively. Haynes® 556® can also withstand higher temperatures for short-time exposures [49]. For the conditioning of the hydrogen and flue gases, SS 316 is replaced by SS 310, which can withstand up to 1150 °C in continuous operation and even higher temperatures for exposures of short duration [48]. For the moving bed heat exchangers, Solex Thermal Science have claimed that their Solex® moving bed can cool bulk solids from up to 2000 °C, with 90% less energy consumption. This technology can treat from 100 to 100,000 kg/h of hot solids indirectly by conduction, and the recovered heat can produce high-grade pressurized steam for their use inside the plant [50,51].

The process flow diagrams of the different cases, along with their mass balances, can be consulted in the Supplementary Material. The list of assumptions for the modeling of the plants is found in Table 2.

Thermodynamic assessment: plant indexes

Thermodynamic assessments have been performed in order to evaluate the global performance of the considered plants for the concept. Different performance indexes were used for the assessment and these indexes were previously explained in the work by Martínez et al. [54]. The mathematical expressions per index can be consulted in Table 3. In order to compare the performance of the new plants with the benchmark technology (SMR), the work done by Spallina et al. [55] was taken as reference for the SMR plants, with and without CCS.

Techno-economic assessment: methodology

The methodology for the cost estimation of power plants developed in 2011 by the US Department of Energy – National Energy Technology Laboratory (DOE-NETL), was the one employed for the techno-economic assessment. The expected accuracy can go from 15 to 30% of underestimation to 20%–50% of overestimation [56].

Total overnight costs

In this methodology, the total capital expenditures are referred to as total overnight costs (TOC), which include the total plant acquisition and installation costs of all the necessary components for the plant. The methodology to calculate the TOC is described in Table 4.

To calculate the bare erected cost per component, Eq. (2) is followed.

Table 2 – General assumptions for the process simulations (taken from [4,52,53]).

Property	Description
NG composition (mol %)	89% CH_4; 7% C_2H_6; 1% C_3H_8; 0.11% C_4H_{10}; 2% CO_2; 0.89% N_2
NG feed conditions	70 bar; 15 °C
NG lower heating value (LHV_{NG})	46.502 MJ/kg
H_2 lower heating value (LHV_{H2})	120.19 MJ/kg
Air composition (mol %) and conditions	77.4% N_2; 20.7% O_2; 1.0% H_2O; 0.9% Ar; at 1 bar and 25 °C
H_2 production capacity	0.75 kg/s (21 kta)
Process Conditions	
Pre-pyrolysis inlet conditions	10 bar; 500 °C
Reactor operating conditions	10 bar; 1200 °C
Burner operating conditions	1 bar; 1250 °C
NG conversion	95% (equilibrium conversion at reactor conditions)
Residence time of the bubbles in the liquid (τ_L)	1 s
Equipment	
PSA inlet conditions	10 bar; 50 °C
PSA H_2 separation purity	99.999%
PSA recovery factor	89%
Steam turbine	30 bar; 366 °C
Isentropic efficiency	94%
CCS CO_2 removal efficiency	90.52%
Electric efficiency in centrifugal pumps	70%
Multi-compressor stages	3
Products Specifications	
Carbon market conditions	1 bar; 30 °C
Hydrogen market conditions	150 bar; 30 °C
CO_2 storage conditions	110 bar; 30 °C
Assumptions made in this work	
Liquid gallium inside the reactor (vol. %)	75% (to reach desired residence time, τ_L)
O_2 in the exhaust gases (mol %):	2% (to minimize excess of air for combustion)

Table 3 – Performance indexes for the thermodynamic assessment of thermal plants (based on [54]).

Index	Mathematical expression	Units
Equivalent natural gas input	$\dot{m}_{NG,eq} = \dot{m}_{NG} - \frac{Q_{th}}{\eta_{th,ref} \cdot LHV_{NG}} - \frac{W_{el}}{\eta_{el,ref} \cdot LHV_{NG}}$	$[kg \cdot s^{-1}]$
Steam export	$Q_{th} = \dot{m}_{steam,export} \cdot (h_{steam@6bar} - h_{liqsat@6bar})$	[W]
H_2 production efficiency	$\eta_{H_2} = \frac{\dot{m}_{H_2} \cdot LHV_{H_2}}{\dot{m}_{NG} \cdot LHV_{NG}}$	[–]
Equivalent H_2 production efficiency	$\eta_{H_2,eq} = \frac{\dot{m}_{H_2} \cdot LHV_{H_2}}{\dot{m}_{NG,eq} \cdot LHV_{NG}}$	[–]
CO2 specific emissions	$E_{CO_2} = \frac{\dot{m}_{CO_2,capt}}{\dot{m}_{NG} \cdot LHV_{NG} \cdot E_{NG}}$	$[kg_{CO_2} \cdot Nm^{-3}_{H_2}]$
Equivalent CO2 specific emissions	$E_{CO_2,eq} = \frac{\dot{m}_{CO_2,capt} - Q_{th} \cdot E_{th,ref} - W_{el} \cdot E_{el,ref}}{\dot{m}_{NG} \cdot LHV_{NG} \cdot E_{NG}}$	$[kg_{CO_2} \cdot Nm^{-3}_{H_2}]$
Equivalent, specific primary energy consumption for CO2 avoided ($SPECCA_{eq}$)	$SPECCA_{eq} = \frac{\frac{1}{\eta_{H_2,eq}} - \frac{1}{\eta_{H_2,eq,ref}}}{E_{CO_2,ref} - E_{CO_2,eq,ref}} \cdot 1000$	$[MJ_{th} \cdot kg^{-1}_{CO_2}]$
Heat Rate (Energy consumption)	$HR_{tot} = \frac{\dot{m}_{NG} \cdot LHV_{NG} - Q_{th} - W_{el}}{\frac{4.186}{\dot{N}_{H_2} \cdot 22.414}}$	$[Gcal_{NG} \cdot kNm^{-3}_{H_2}]$

$$C_i = C_0 \cdot \left[\frac{S}{S_0}\right]^f \cdot \frac{CEPCI_{2019}}{CEPCI_{year}} \quad (2)$$

A scaling parameter C_0 of a reference equipment of size S_0 is required for calculating the actual erected cost, C_i, for an equipment of size S. Moreover, a scaling factor f is employed, which depends on the type of equipment. Inflation is included in the ratio of the Chemical Engineering Plant Cost Indexes (CEPCI) between 2019 and the year of estimation of the scaling parameter. The scaling parameters and factors were taken from literature. For the cases in which the scaling factor f was not given, the "six-tenth rule" was considered (i.e. 0.60) [58]. This heuristic gives satisfactory results when the permissible error in the cost estimation is ±20%, which applies in this methodology. Finally, to convert US dollars to euros, a conversion factor of 0.88 €/$ (May 2020) was used. The relevant information for the TBEC calculation is presented in Table 5.

The costing of the reactor was done differently due to its premium construction material. The cost of 602CA® alloy may vary from 30 to 40 €/kg. An article from Industrial Heating magazine reported an approximate value of 20.85 $/lb (i.e. 46 $/kg) [65]. A value of 40 €/kg was used in the cost estimation. The total weight of the vessel depends on its thickness. The thickness of the vessel for a design pressure of 15 bar and 1200 °C was determined as proposed by Ulrich and Vasudevan [66]. The total weight of metal needed for the reactor was then calculated and material price was applied to obtain the material costs. A correlation found in Walas [67] was chosen for calculating purchased costs for vertical vessels. The purchased costs were given for 1985, and these were updated to 2019 by using the ratio between CEPCIs.

Fixed and variable operating & maintenance costs ($C_{O\&M,fixed}$/ $C_{O\&M,variable}$)

The $C_{O\&M,fixed}$ and $C_{O\&M,variable}$ are the major components of the total operating expenditures (OPEX). On the one hand, the $C_{O\&M,fixed}$ is a non-temporal cost and it depends on the TOC. On the other hand, the $C_{O\&M,variable}$ is time-dependent because it is affected by the capacity factor of the plant. Carbon production is included as revenue, which is expressed by a minus sign. Table 6 presents the operating costs considered for the process.

Levelized cost of hydrogen & cost of CO_2 avoided

The so-called levelized cost of hydrogen (LCOH) is the final value after the techno-economic assessment for hydrogen production plants. It is assumed that the LCOH is constant over the plant lifetime [56]. The cost of CO_2 avoided (CCA) determines how much money is required to invest per unit mass of CO_2 captured for the implementation of a CCS unit, excluding transportation and storage costs. The equations for calculating both LCOH and CCA are given in Eqs. (3) and (4), respectively.

$$LCOH\left[\frac{€}{kg_{H_2}}\right] = \frac{(CCF \cdot TOC) + C_{O\&M,fixed} + (C_{O\&M,variable} \cdot h_{eq})}{H_{2,prod} \cdot h_{eq}} \quad (3)$$

where:

$$CCA\left[\frac{€}{t_{CO_2}}\right] = \frac{[(CCF \cdot TOC)_{CCS} - (CCF \cdot TOC)] + [C_{O\&M,fixed,CCS} - C_{O\&M,fixed}] + [(C_{O\&M,variable} \cdot h_{eq})_{CCS} - (C_{O\&M,variable} \cdot h_{eq})]}{(\dot{m}_{CO_2,emitted} - \dot{m}_{CO_2,emittedafterCCS}) \cdot h_{eq}} \quad (4)$$

Table 4 – TOC calculation methodology (adapted from [57]).

Plant Component	Costs
Total Bare Erected Costs (TBEC)	$C_1 + C_2 + C_3 + C_4 + \ldots + C_n$
Direct costs as percentage of the TBEC: Piping/valves, Civil works, Instrumentation, Steel-Structure, Erection, etc.	
Total Installation Costs (TIC)	80% TBEC
Total Direct Plant Costs (TDPC)	TBEC + TIC
Indirect Costs (IC)	14% TDPC
Engineering, Procurement and Construction Cost (EPCC)	TDPC + IC
Contingencies & Owner's Costs (C&OC)	
Contingency	10% EPCC
Owner's cost	5% EPCC
Total C&OC	15% EPCC
Total Overnight Costs (TOC)	**EPCC + C&OC**

TOC: total overnight costs [€];
CCF: first year capital charge factor [$year^{-1}$];
$C_{O\&M,fixed}$: fixed, operating and maintenance costs [€.$year^{-1}$]; $H_{2,prod}$: production of hydrogen [kg.h^{-1}];
$C_{O\&M,variable}$: variable, operating and maintenance costs [€.h^{-1}]; h_{eq}: Equivalent working hours [h.$year^{-1}$];

The CCF refers to the finance structure considered for the estimation. There are two types of finance frameworks: Investor-Owned Utility (IOU) and Independent Power Producer Developer/Owner (IPP). These could be individually considered with low or high risk. IPP was chosen with a low risk assessment, meaning that the CCF value is 0.149 $year^{-1}$, as indicated in the DOE-NETL report [56]. The equivalent working hours were assumed to be 7884 h $year^{-1}$, which implies that the process works continuously 90% of the year, and the remaining 10% is directed to maintenance, renovation of the molten metal or scheduled shutdowns.

Results & discussions

Methane pyrolysis with and without molten gallium

The thermal cracking of methane was validated experimentally using molten gallium in a quartz reactor with a microporous distributor. Carbon was deposited on top of the molten metal's surface, and its segregation from the gas phase was gradually improved as more gallium was added to the reactor. For the experiments using empty reactors, the gas residence time was estimated to be 13-10 s for the temperature range 900–1100 °C. After experimentation, considerable amounts of solid carbon were found on the reactor walls. Same observation was found at the upper part of the reactor when using molten gallium. This suggests that either gas-phase thermal cracking occurred after the unconverted methane left the molten metal, or a portion of carbon deposited on the metal surface was dragged by the gas and accumulated on the walls, or a combination of the two. However, the amount of carbon was significantly lower than that for empty reactors and clogging of the outlet pipes by carbon deposition did not occur. This allowed operation times higher than 40 min, which was the maximum achievable for the empty reactors (blank experiments). The conversion of methane as a function of the average reaction temperature for the blank experiments and those with molten gallium are presented in Fig. 5. Moreover, images taken from the top view of the reactor, before and after pyrolysis for the experiments with molten metal were included.

As seen in Fig. 5, relatively high conversions were achieved by the increase in temperature for all experiments. Nevertheless, the actual conversion values were significantly lower than those at equilibrium conditions (see Fig. 1). Temperature maldistributions along the height of the reactor were generally found in the experiments. The biggest differences in temperatures were registered after 1050 °C, with values differing from one another approximately 30–35 °C. The high operating temperatures and the lack of perfect isolation of the experimental setup are responsible for these variations. Nevertheless, the temperature inside the reactor was not constant, hampering a correct estimation for the actual cracking temperature. Moreover, quartz does not transfer heat as effective as metals. This lack of temperature homogeneity also affected the achieved conversions. This rapid fluctuation was seen despite being the thermocouples only separated by 16 cm. Regarding the blank experiments, a minimum methane conversion of 36% is achieved at the lowest investigated temperature (932 °C), however this conversion value is almost doubled by a temperature increase of only 10 °C, which suggests that the reaction was not fully performed for this data point. For the set of experiments with

Table 5 – Referenced parameters for the cost estimation of the TBEC ($CEPCI_{2019}$ = 607.5).

Equipment	Scaling Parameter	S_0	C_0 (M€)	f	Cost Year	CEPCI Year	Ref.
Air blower	Power (MWe)	1	0.23	0.67	2006	499.6	[59]
Burner	Vessel volume (m^3)	81.3	0.16	0.60	2016	541.7	[4]
Centrifugal Pump	Power (kW)	197	0.12	0.67	2009	521.9	[60]
CO2 compressor	Compressor power (MWe)	13	9.95	0.67	2011	585.7	[57]
Electric Arc Furnace	Net electric power (MWe)	175	44	0.60	2016	541.7	[4]
H2 compressor	Compressor power (MWe)	1	0.0012	0.82	1987	323.8	[61]
Heat Exchanger	Duty (MMBTU/h)	659.9	10.84	0.60	2006	499.6	[62]
MEA CCS Technology	CO_2 captured flow (kg/s)	38.4	28.95	0.80	2011	585.7	[57]
PSA Unit	Purge gas flow (kmol/s)	0.294	6.25	0.74	2002	395.6	[63]
Steam turbine & condenser	Turbine gross power (MWe)	136	52.1	0.67	2002	395.6	[63]
Solex® Heat Exchanger	Solids Capacity (t/h)	1195	9.06	0.60	2016	541.7	[64]

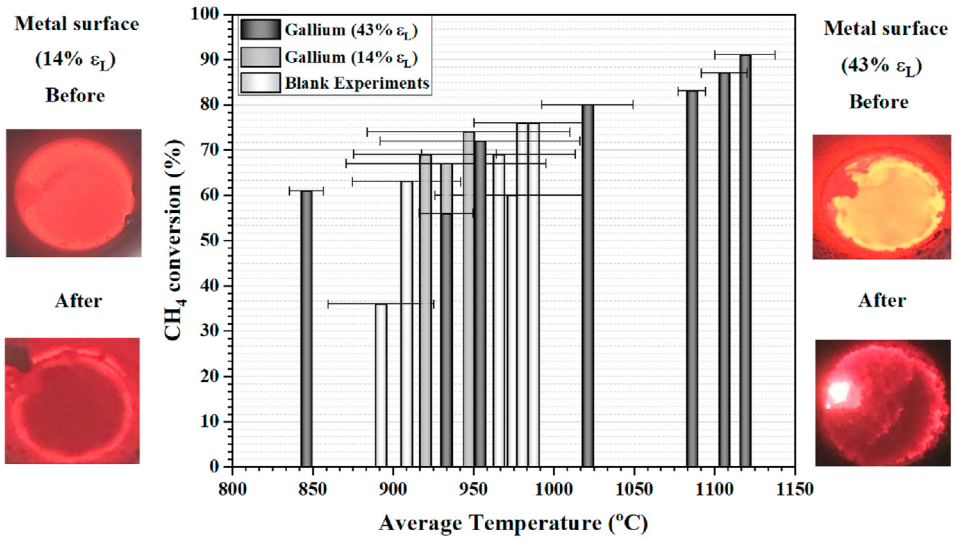

Fig. 5 – Evolution of methane conversion with reactor temperatures, for blank and gallium experiments. Images taken from the top-view of the reactor before and after the cracking reaction.

gallium, the τ_L in our reactor was calculated following the same approach as proposed by Andreini et al. [36], for gas bubble velocity determination under laminar flow conditions in molten metals. The average residence time of the bubbles in the molten metal was 0.25 and 0.65 s for the 14% and 43% gallium filling experiments, respectively. The experiments with 14% of gallium filling yielded conversions in the order of 69–74% at the temperature interval 960–995 °C. As a result, a high amount of carbon was deposited at the top of the molten gallium, as shown in Fig. 5. Concerning the experiments with 43% of gallium filling, which is more than 3 times higher than the latter, more than 80% of the fed methane is converted into hydrogen above 1000 °C. Reaction temperatures higher than 1050 °C were only achieved for this set of experiments. This is explained due to the high heat storage capability of gallium, which ensures a more homogeneous temperature profile for the reaction. As a consequence, less fluctuations in the registered temperatures are found because less heat is dissipated away from the reactor, resulting in higher conversions. The highest methane conversion of the study (91%) was reached at a temperature of 1119 °C. The temperature homogeneity improves the conversion of the latter around 2–10%, highlighting the importance of a suitable temperature control at the industrial scale concept that must be followed in order to not lose productivity. After pyrolysis, the stratification of different carbon layers on top of the molten metal was clearly visible. This provides useful insights of how this process might behave at industrial scale and how carbon should therefore be separated from the molten media. Regarding the comparison with empty reactors, similar methane conversions were achieved when gallium was used. However, the residence time of the gas in blank experiments was in the order of 10–13 s whereas the mean gas residence time in the metal was below 1 s for all cases. This suggests that gallium may present catalytic properties for methane pyrolysis, besides providing enhanced temperature homogeneity inside the reactor. However, this requires further investigation before validation. A comparison in performance between the previously mentioned LMBCR works and our reactor concept is presented in Table 7.

Concerning the type of gas distributor, higher methane conversions were achieved by using a quartz microporous plate than for the ones which distribute the gas through a single orifice. The τ_L values for the reactors with 0.5- and 1-

Table 6 – Assumptions for the calculation of $C_{O\&M,\ fixed}$ and $C_{O\&M,variable}$.

$C_{O\&M,fixed}$	Cost	Units	References
Labor costs	1.50	M€	[55,68]
Maintenance cost	2.50	% TOC	[55,68]
Insurance	2.00	% TOC	[55,68]
$C_{O\&M,variable}$	Cost	Units	References
Natural gas	0.425	€/kgNG,LHV	[55]
Cooling water	0.35	€/m^3	[55,57,69]
Process water	2.00	€/m^3	[55,69]
Electricity	76.36	€/MW.h	[55]
Gallium Metal (Rotterdam, 2020)	141	€/kg	[70]
Carbon Tax	50	€/tCO2,emitted	
Carbon black (USA, mid-2018)	- 296	€/t	[71]

Table 7 – Performance of our reactor concept with respect to previous works concerning LMBCRs.

Source	Bubbles generator	MM	τ_L (s)	Temperature (°C)	CH_4 Conversion (%)
Serban et al. [10]	MOTT® 0.5 μm porous distributor	Tin	0.5–0.3	750	51
Plevan et al. [32]	1 mm orifice	Tin	2.7–1.7	900	18
Geißler et al. [33]	0.5 mm orifice	Tin	4.9–3.2	1000	32
This work	DURAN® 0.2 mm porous distributor	Gallium Gallium	0.3–0.2	960–995	69–74
			0.8–0.5	936–1119	61–91

mm orifices (4 and 2 s, respectively) were significantly higher than determined in this work, with average values of 0.3 and 0.7 s at 14% and 43% gallium fillings, respectively, although this did not translate into higher conversions. The enhanced performance of our reactor concept is due to the high gas-liquid interfacial areas achieved by the porous distributor, which is the key parameter in bubble columns. However, comparing the LMBCRs which use porous gas distributors, different conversions were achieved at similar values of τ_L. One reason is the difference in reaction temperatures. The higher the reaction temperature, the higher the intrinsic kinetics. A second reason is the use of an inert to the feed. Serban et al. [10] achieved 51% conversion with pure tin at 750 °C without inerts present in the feed, whereas our molten gallium reactor achieved 91% of methane conversion at 1119 °C using a diluted feed with Argon. The use of an inert reduces the partial pressure of methane for the reaction, and the equilibrium is shifted towards hydrogen production following Le Châtelier's principle. To sum up, methane pyrolysis was satisfactory in this work mainly due to the use of gallium, which ensured good temperature distribution and plausible catalytic properties for the reaction; and the use of a porous plate for efficient bubble distribution which allowed high surface areas for the cracking reaction.

Carbon quality assessment

Raman spectroscopy

In order to determine the type of carbonaceous material, a comparison of two Raman spectra was made. The first one corresponded to that for the carbon samples of this work, whereas the second one corresponded to the Raman spectra which is similar to the one for the samples. This similar spectra was found for carbon black, and it was taken from the work done by Bokobza et al. [72]. Both spectra are presented in Fig. 6.

Two characteristic peaks were observed in both spectra within the Raman shift range of 1300–1600 cm^{-1} reported in Fig. 6. These peaks were found at 1340 and 1581 cm^{-1}, respectively. In fact, the 1340 cm^{-1} peak belongs to the so-called diamond band (D), whereas the peak at 1581 cm^{-1} shows the graphite band (G). The D band generally accounts for structural defects, meaning that a high intensity of this band shows an irregular carbon structure. For example, this band is very weak for high-quality graphene, which is a highly ordered material with low number of defects. The ratio of intensity between the D and G bands gives an indication about the defects present on the carbon structure [73]. The D/G intensity ratio for the carbon samples was 1.02, fairly similar to the 1.16 registered by Bokobza et al. [72]. This means that the structure is highly disordered, which does not correspond to graphene, but to a more amorphous structure, such as carbon black (CB). Both figures match at great extent and therefore it is concluded that the obtained carbon from the pyrolysis reaction is carbon black, which is a valuable material with many applications in the rubber tire industry [16].

BET surface area

Four different carbon powders, according to their formation temperature, were analyzed in order to determine the effect of temperature on the BET surface area and mean pore size. The results are presented in Table 8.

In Table 8 it is remarkable the low BET surface area values of the carbon black samples for all the range of formation temperatures. All surface areas were below 5 m^2/g, independent from the considered formation temperatures, which is a value 16 times lower than that for average carbon black (60–80 m^2/g). This can be explained by the rapid formation of

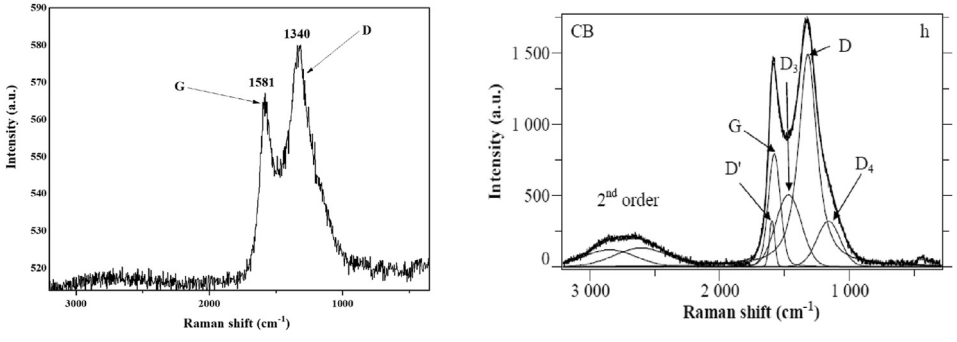

Fig. 6 – Raman Spectra for (a) carbon samples (b) carbon black (taken from [72]).

Table 8 – BET surface areas and mean pore sizes of the carbon samples at different formation temperatures.

Carbon Powder	BET Surface Area (m^2/g)	Mean Pore Size (nm)
950 °C	3.58	6.91
1000 °C	2.92	6.79
1030 °C	3.35	6.88

this carbon in the reactor. Geißler et al. [33] also determined BET surface areas that were lower than the average, with values ranging from 8 to 23 m^2/g. Furthermore, other authors reported that carbon black, produced at 10 s of residence time and temperatures 1200–1350 °C, presented a BET surface area of 8 m^2/g [74]. It is concluded that carbon produced by methane pyrolysis possesses no catalytic properties and cannot be sold as activated carbon or similar materials. The produced material can be characterized as non-adsorptive, nanoporous carbon black and will be used in the cost analysis for the next sections.

Thermodynamic assessment of the case scenarios for the industrial process

The thermodynamic assessment of the considered cases for the thermal decomposition of natural gas (TDNG), was performed and compared with the one made by Spallina et al. [55], who made the assessment of the SMR process with and without CCS technology. To compare the different technologies, the same H_2 production capacity reported in said work was selected for the TDNG plants. The results are presented in Table 9.

In Table 9, a wide range of information is found for the technologies concerning process specifications, electricity demands, and efficiency studies of H_2, NG and CO_2 for each plant, in order to assess their global performance. Regarding process input specifications, it is noticeable that all TDNG cases require more NG than that of the benchmark technology. This is because the theoretical global production is 4 mol_{H2}/mol_{NG} for SMR, whereas the maximum for methane pyrolysis is only half of it. Although cases 1, 3 and 4 require the same NG input for the reactor, case 3 requires an additional input of NG to be used as fuel for the burner. Case 2 demands the highest amount of NG due to the partial use of H_2 as energy source for the reactor, implying more NG in the feed to meet the H_2 capacity. In fact, the amount of NG needed in case 2 (7.31 kg/s) is almost three times the amount of SMR, implying higher operating costs.

In terms of power demands, the amount required by the H_2 compressors for cases 1–3 is significantly higher than that for SMR, due to the fact that hydrogen is produced at 10 bar, instead of 32 bar as in SMR. In Case 4, the electric arc furnace has the biggest power demands (15.85 MW_e), requiring nearly 4 times more than that to compress hydrogen. Regarding the CCS scenarios, power demands for CO_2 compression in cases 1 and 3 are lower than that for the benchmark with CO_2 capture. This is due to the fact that the amount of CO_2 produced by the combustion of carbon black or natural gas is not as high as the amount produced in the benchmark process, highlighting the benefit of producing hydrogen from TDNG. Steam is not exported in the TDNG cases because is completely used for in-situ electricity supply to the process. For TDNG cases 1 to 3, this supply is sufficient, and the remaining part can be exported, however for case 4 an additional amount needs to be purchased from the general electricity grid, due to the high demands of the furnace.

Regarding the plant indexes, the lowest equivalent H_2 production efficiency is found in Case 2 (30%), because it requires the highest NG input of all considered plants. Conversely, the highest efficiency is found in SMR without CCS, because the H_2 yield is also the highest one of all processes, with 2.49 $mol_{H2}/mol_{,eq,CH4}$. In addition, the equivalent heat rate consumptions of the benchmark with and without capture (<43 $Gcal/t_{H2}$) are lower than those for the TDNG cases, because the equivalent amounts of NG to be fed into the process are also the lowest. The heat rate values for the TDNG are sensitively higher, and naturally the highest is found for the process with the highest NG demand for the pyrolysis (Case 2), whereas the lowest value is found in Case 4 (54.2 $Gcal/t_{H2}$). In contrast, the benchmark is last in line when it comes to the abatement of CO_2 emissions. Comparing the processes without CCS, SMR emits nearly twice as much CO_2 as cases 1 and 3. Equivalent net CO_2 emissions are negative when burning hydrogen or using electricity to supply heat to the reactor, implying a direct benefit to the environment. In Case 4, CO_2 is emitted in these cases by the combustion of the off-gas stream of the PSA unit for hydrogen purification, but also important amounts of power are produced, resulting in a net negative carbon footprint. Concerning the CCS scenarios, again the SMR is less efficient in terms of CO_2 avoided (79%), behind the TDNG cases with capture efficiencies over 90%. Finally, the $SPECCA_{eq}$ index refers to the same process with and without capture and is strongly affected by the loss in H_2 efficiency when implementing the CCS technology in the process. For the TDNG cases, this efficiency loss is not as high as that for SMR, resulting in a lower $SPECCA_{eq}$ value, meaning that the energy requirements to capture CO_2 are also lower. To sum up, case 2 is the best scenario in terms of CO_2 abatement, but the worst one when referring to hydrogen efficiency, NG input or Heat Rate values. Cases 1, 3 and 4 are in between in terms of productivity, efficiency and CO_2 capture. A techno-economic assessment of the cases is thus necessary to determine the competitiveness of these TDNG processes with respect to the benchmark.

Techno-economic assessment

The results of the techno-economic assessment for all TDNG cases, and the ones obtained by Spallina et al. [55] for the benchmark processes, are presented in Table 10. The base case consisted of a NG price of 0.425 €/kg, a carbon sale price of 296 €/t, a carbon tax of 50 €/t_{CO2} and an electricity price of 76.36 €/MW.h. Moreover, the lifetime of gallium was set to 1 year, based on the fact that gallium is highly stable, and it is not expected to be consumed or wasted during the process.

Table 9 – Thermodynamic performance of the scenarios and comparison with the benchmark process.

Process	Benchmark: SMR [55]		TDNG: Case 1		TDNG: Case 2	TDNG: Case 3		TDNG: Case 4
CO_2 Capture	N/A	CA-MDEA	N/A	CA-MEA	N/A	N/A	CA-MEA	N/A
T_{ref} [°C]/P_{ref} [bar]	890/32	890/32	1200/10	1200/10	1200/10	1200/10	1200/10	1200/10
NG flow rate [kg/s]	2.62	2.81	3.86	3.86	7.31	5.33	5.33	3.86
NG thermal input [$MW_{LHV,NG}$]	121.94	130.79	179.55	179.55	339.72	247.88	247.88	179.55
Steam-to-carbon ratio (SC)	2.7	4.0	0.0	0.0	0.0	0.0	0.0	0.0
H_2 mass flow rate [kg/s]	0.75	0.75	0.75	0.75	0.75	0.75	0.75	0.75
Power breakdown and plant indexes								
Air blower [MW_{el}]	−0.68	−0.91	−0.32	−0.32	−0.68	−0.60	−0.60	−0.13
H_2 compressors [MW_{el}]	−2.27	−2.28	−4.21	−4.21	−4.21	−4.21	−4.21	−4.21
CO_2 compressors [MW_{el}]		−2.23		−1.61			−1.91	
Steam Turbine (s) [MW_{el}]	3.27	3.79	10.93	10.93	27.55	19.39	19.39	10.96
Pumps [MW_{el}]	−0.21	−0.29	−0.07	−0.07	−0.18	−0.12	−0.12	−0.07
Other Auxiliaries [MW_{el}]	−0.05	−0.15						−15.85
Net electric power [MW_{el}]	0.07	−2.07	6.33	4.72	22.48	14.46	12.56	−9.30
Steam export (160 °C, 6 bar) [kg/s]	4.02	0.27						
H_2 efficiency, η_{H2} (H_{2LHV}/NG_{LHV})	0.74	0.69	0.50	0.50	0.27	0.36	0.36	0.50
Eq. NG input, $m_{NG,eq}$ [kg/s]	2.41	2.88	3.63	3.69	6.48	4.80	4.58	3.52
H_2 yield ($mol_{H2}/mol,eq,_{CH4}$)	2.49	2.48	1.65	1.63	0.93	1.25	1.23	1.71
Eq. H_2 efficiency, $\eta_{H2,eq}$ (H_{2LHV}/NG_{LHV})	0.81	0.67	0.54	0.53	0.30	0.40	0.40	0.55
Heat Rate [Gcal/t_{H2}]	36.3	42.4	55.1	55.7	101	74.3	74.9	54.2
CO_2 spec. emissions, E_{CO2} [kg_{CO2}/kg_{H2}]	9.18	1.57	5.26	0.45	1.46	6.16	0.56	1.01
Eq. CO_2 spec. emissions, $E_{CO2,eq}$ [kg_{CO2}/kg_{H2}]	8.51	1.79	4.37	−0.11	−1.46	4.37	−1.01	−0.22
Eq. CO_2 avoided [%]								
(ref. = SMR w/o CCS)		79	49	101	117	49	112	103
(ref. = Case w/o CCS)				103			123	
$SPECCA_{eq}$ [MJ/kg_{CO2}]								
(ref. = SMR w/o CCS)		4.57						
(ref. = Case w/o CCS)				0.94			0.23	

The carbon tax used for the TDNG cases was also applied for the SMR processes, implying higher LCOH values than those reported by the above-mentioned authors, because they did not consider any penalty for emitting CO_2 from their plants. Considering the TBEC, it is evident that for the TDNG cases the major costs are caused by the equipment needed for power production and heat integration, accounting for 60–85% of the TBEC. This distribution differs from the SMR process, wherein the reformer, WGS reactor and PSA unit account for almost 50% of the TBEC. For instance, the steam turbine in Case 2 represents almost 60% of the capital costs. In Case 4, the cost of the electric arc furnace represents more than 25% of the TBEC, and this equipment is more expensive than all the required heat exchangers together. Moreover, hydrogen compressors represent an average value of 7%, mainly due to the high-pressure specifications for the final H_2 product (150 bar). In the TDNG cases with carbon capture, extra costs are coming from CO_2 compressors (5–7%) and the CCS technology (11–12%), the latter being half of the share of the equivalent CCS technology for the SMR process. The reactor and burner represent less than 4% for all cases, since they are merely process vessels.

The (TOC x CCF) and $C_{O\&M,fixed}$ are slightly lower for the TDNG cases than those for the benchmark processes. Specifically, these two values are within the range 10.60–16.64 and 4.70–6.52 M€/year for the TDNG cases, respectively. For SMR with and without CCS, (TOC x CCF) values are 21.70 and 14.15 M€/year; whereas $C_{O\&M,fixed}$ values are 9.75 and 6.60 M€/year, respectively. The low CO_2 production and high hydrogen purity achieved by the TDNG processes decrease the TOC, as much smaller equipment is needed for the capture and separation steps. Regarding the variable costs, the differences are much higher. The higher equivalent hydrogen efficiencies achieved by the SMR processes require the lowest NG inputs, implying that around 31–34 M€ in NG would be spent yearly for this concept. When comparing these costs with Cases 1 and 4, which use the lowest NG inputs, the yearly cost is nearly 13 M€ more; and for Cases 3 and 2, these costs are almost doubled and tripled, respectively. Another major expense is the molten metal acquisition. For a molten gallium lifetime of 1 year, 12–25 M€ would be spent in this concept, representing 20–25% of the total variable operating costs. This increment clearly demonstrates that, in terms of hydrogen yield, TDNG processes cannot merely compete with SMR. Co-product carbon must be sold in order to make TDNG processes economically feasible. Concerning carbon tax, SMR is clearly affected by this penalty. By using 50 €/t_{CO2}, which is an expected value in the upcoming years due to acute environmental restrictions, the carbon tax in the non-capture process represents almost one third of the NG yearly costs. This cost is reduced in the TDNG because the associated CO_2 emissions are sensitively lower, and the final share is not above 7.5% for all cases. Regarding electricity demands, only Case 4 is clearly dependent on the general grid price, as the electric arc furnace requires enormous amounts of electricity in a yearly basis. Electricity costs are over 8%, whereas for the remaining TDNG

Table 10 – Cost breakdown of the capital, operating expenses and final LCOH for each case study.

Process	SMR		Case 1		Case 2	Case 3		Case 4
CO_2 capture technologies	N/A	CA-MDEA	N/A	CA-MEA	N/A	N/A	CA-MEA	N/A
T (°C)/P (bar)/SC (–)	890/32/2.7	890/32/2.7	1200/10/-	1200/10/-	1200/10/-	1200/10/-	1200/10/-	1200/10/-
H2 mass flow rate [kg/s]	0.75	0.75	0.75	0.75	0.75	0.75	0.75	0.75
Marketable Carbon [t/h]			6.20	6.20	17.94	9.30	9.30	9.30
BEC [M€] (% of TBEC)								
Reactors	10.56 (27.3%)	11.11 (18.7%)	0.82 (2.7%)	0.82 (2.2%)	1.65 (3.5%)	0.82 (2.2%)	0.82 (2.1%)	0.82 (1.9%)
Heat Exchangers	14.84 (38.3%)	19.85 (33.4%)	8.31 (27.6%)	8.31 (22.4%)	11.39 (24.1%)	10.38 (26.4%)	10.38 (21.9%)	9.46 (22.1%)
Steam turbine & condenser	3.42 (8.8%)	3.70 (6.3%)	14.78 (49.0%)	14.78 (39.8%)	27.45 (58.0%)	21.70 (55.1%)	21.70 (45.9%)	14.80 (34.5%)
H_2 compressors	1.46 (3.8%)	1.38 (2.3%)	2.68 (8.9%)	2.68 (7.2%)	2.68 (5.7%)	2.68 (6.8%)	2.68 (5.7%)	2.68 (6.3%)
PSA unit	8.45 (21.8%)	5.9 (10.0%)	3.16 (10.5%)	3.16 (8.5%)	3.45 (7.3%)	3.16 (8.0%)	3.16 (6.7%)	3.16 (7.4%)
MDEA unit		14.29 (24.1%)						
MEA unit				4.47 (12.0%)			5.12 (10.8%)	
CO_2 compressors		3.12 (5.2%)		2.55 (6.9%)			2.84 (6.0%)	
Burner, pumps, air blower			0.41 (1.3%)	0.41 (1.1%)	0.69 (1.5%)	0.60 (1.5%)	0.60 (1.3%)	0.28 (0.7%)
Electric arc furnace								11.68 (27.2%)
TOC x CCF [M€/y]	14.15	21.70	10.60	13.07	16.63	13.83	16.64	15.08
$C_{O\&M,fixed}$ [M€/y]	6.60	9.75	4.70	5.45	6.52	5.68	6.52	6.05
$C_{O\&M,variable}$ [M€/y]								
Water (process + cooling)	0.63	0.82	2.11	2.11	2.57	2.73	2.73	2.25
Natural Gas	31.67	33.97	46.57	46.57	88.12	64.30	64.30	46.57
Electricity	−0.02	1.14	−3.81	−2.84	−13.53	−8.71	−7.56	5.60
Gallium Metal			12.34	12.34	25.65	12.34	12.34	12.34
Carbon Tax	9.86	1.51	5.56	0.53	1.56	6.60	0.63	1.08
Carbon revenues			−14.45	−14.45	−41.81	−21.68	−21.68	−21.68
LCOH [€/kg_{H2}]								
LCOH, $_{variable}$	1.91	1.76	2.22	2.08	2.94	2.61	2.38	2.17
LCOH, $_{fixed}$	0.95	1.60	0.72	0.87	1.09	0.92	1.09	0.99
LCOH, $_{total}$	2.86	3.36	2.94	2.95	4.03	3.53	3.47	3.16
CCA [€/t_{CO2}]								
(ref. = process w/o CCS)		35.94		−8.40			−9.91	
Eq. CCA [€/t_{CO2}]								
(ref = process w/o CCS)		41.60		−8.92			−10.20	

cases, electricity can be exported, increasing the revenues of the processes.

Regarding LCOH, the lowest is encountered in the benchmark process without capture (2.86 €/kg_{H2}), closely followed by Case 1 (2.94 €/kg_{H2}) and Case 4 (3.16 €/kg_{H2}). The highest is reached in Case 2, as consequence of using the highest NG input of the study. These hydrogen production costs are higher than those commonly estimated, and this is due to the economy of scale. Capacities of large-scale commercial plants for H_2 are designed for 100–200 kta H_2 production, which is nearly 5–10 times the plant size considered in this work.

Looking at the CCA, the highest value is found for the SMR with capture, which is clearly affected by the implementation of a big, costly CCS technology. Negative values are found in Cases 1 and 3 with capture, which means that the addition of a CCS plant is not as expensive as to pay for the carbon tax. In Case 1 without capture, the economics are promising because the applied carbon tax is almost half the amount for SMR, and also because the increase in NG input is compensated by the revenues obtained from the sale of carbon. Costs for transport and storage of CO_2 were not considered, since they do not depend on the capture technique. However, transport and storage costs should be included in more rigorous estimations for large scale plants, as they may represent 1–4 and 6–13 USD/t_{CO2}, respectively, depending on the power plant distance to the storage site and the considered storage site [57]. At this point, it is important to mention that the carbon black sale price proposed for the study (i.e. 296 €/t) is considered to be a conservative value, lower than those proposed by Keipi et al. [75] (500–4000 €/t) and by Muradov and Veziroğlu [12] (1100 €/t). If TDNG technology were to be implemented at large scale, enormous amounts of carbon black would also be co-produced, and eventually carbon black prices would decrease (effects on market prizes have not been taken into account here). By increasing slightly the carbon sale price, lower LCOH values are expected for all TDNG cases. To conclude, Case 1 with and without carbon capture and Case 4 have shown to be economically feasible and can compete with the benchmark process while being a greener, more sustainable alternative for H_2 production.

Sensitivity analyses

Several sensitivity analyses were performed for those key parameters with direct effect on the final LCOH, for all considered scenarios. The reference LCOH value for each sensitivity analysis was that for SMR without CCS. The selected parameters were the NG acquisition price, molten metal lifetime, the carbon selling price, the carbon tax and the cost of electricity. The acquisition price for natural gas was varied from 0.19 to 0.29 and 0.39 €/kgNG, which corresponds to the actual trend (until 2030) for NG price in USA, Europe and Japan, respectively [76]. Moreover, a pessimistic scenario of

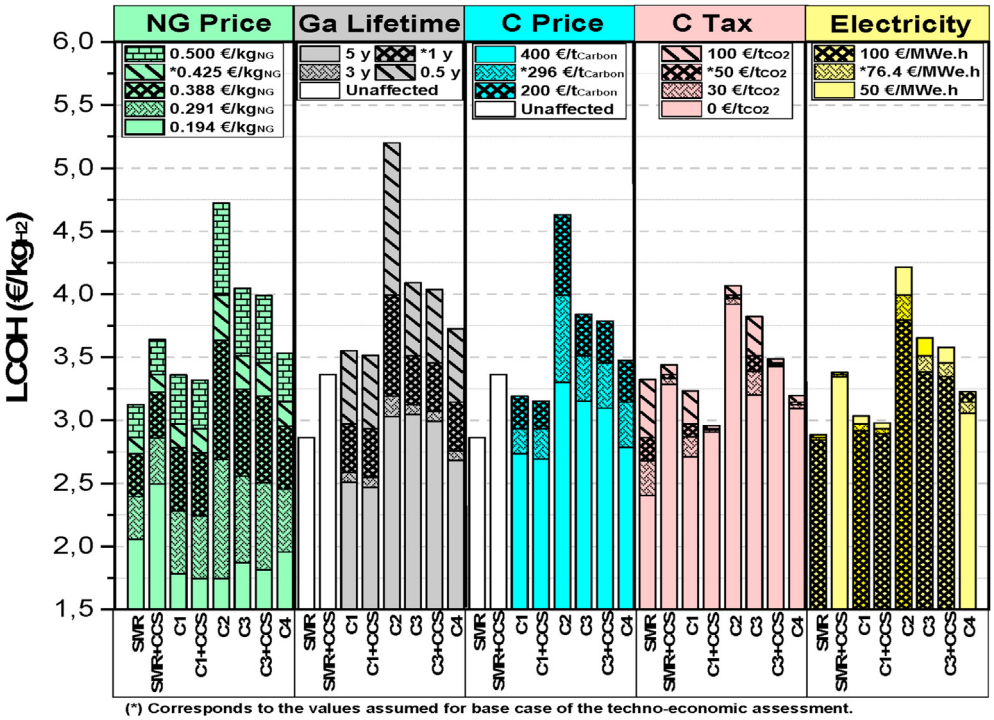

Fig. 7 – LCOH of the case scenarios proposed in the sensitivity analyses for a hydrogen capacity of 21 kta.

0.50 €/kgNG was considered. The lifetime was varied from 1 to 3 and 5 years, for more optimistic scenarios, and 6 months for a more pessimistic approach. Furthermore, carbon sale price was varied in the range 200–400 €/t, providing that the quality of the carbon is high enough to be sold as a sulfur and ash-free premium substitute for petroleum coke [12]. Finally, carbon tax was varied from 0 to 100 €/tCO2 and the electricity, from 50 to 100 €/MW.h. The results of these sensitivity analyses are shown in Fig. 7.

The figure shows that there are 4 new LCOH values as a result of the variation in the NG price. If the NG price drops up to 0.194 €/kg, all the TDNG cases can produce hydrogen cheaper than the benchmark technologies. At 0.291 €/kg, all cases are still competitive excepting Case 2, which is critically affected by this change of price. At more expensive NG prices, only Cases 1 and 4 are robust enough to be competitive with the benchmark processes. This is expected because both cases required the lowest NG inputs, and their economics are less affected by a rapid fluctuation of the NG prices. However, Case 4 produces more expensive hydrogen than Case 1, with an average increase of 0.2 €/kg. The high electricity demands of Case 4 is responsible for this increment. Regarding molten metal lifetime, it is also remarkable its effect on the LCOH. For the least favorable scenario all cases increase their LCOH, with respect to the lifetime for the base case, around 0.5–0.7 €/kg_{H2}, excepting Case 2 with a rise close to 1.2 €/kg_{H2}. This high increment is because more gallium would have to be bought, and in this process the reactor is the biggest one among the TDNG cases. Thus, Case 2 would never be competitive under these circumstances. Furthermore, for a lifetime of 3 and 5 years, lower LCOHs are obtained for Cases 1 and 4 than those for the benchmark processes, which are unaffected by this property. The sensitivity analysis of the carbon sale price reflects an interesting insight. By selling the carbon at the lower bound of 200 €/t, Case 1 with and without capture produce cheaper hydrogen than that for the benchmark with CCS, and Case 4 is competitive under this pessimistic scenario. By doubling the sale price of carbon, all the technologies are competitive with the benchmark process with CCS, and Case 2 obtains the biggest reduction in LCOH, from 4.6 to 3.3 €/kg_{H2}.

Analyzing the carbon tax, it is evident that its absence benefits the SMR process because it emits more CO_2. However, an increase in its value strongly affects the benchmark. In fact, the LCOH rises from 2.3 to 3.3 €/kg_{H2} when carbon tax goes from 0 to 100 €/t_{CO2}. Under this high carbon taxes, Cases 2 and 3 without CCS are not competitive at all due to their lower H_2 efficiencies, even though their CO_2 emissions are also lower than those for SMR. Case 1 without CCS is highly competitive because of its moderately high hydrogen efficiency and also because it releases almost half of the emissions of SMR. Finally, and regarding the effect of electricity on LCOH, Cases 2, 3 and 4 are significantly affected by it. This is logical because Cases 2 and 3 exports high amounts of electricity, and a reduction of its sale price decreases the revenues of the plant. For Case 4, the opposite effect occurs because electricity needs to be imported at lower costs.

Conclusions

Molten metal-based processes for natural gas decomposition offer the generation of hydrogen with carbon segregation in

the absence of atmospheric CO_2 emissions. In this concept, pyrolysis of methane was achieved by using molten gallium inside a quartz bubble column with a porous plate distributor. A maximum methane conversion of 91% was accomplished in a 50-50% Ar-CH_4 mixture at an average reactor temperature of 1119 °C, where gallium represented 43% of the total reactor volume. Methane conversion was improved by increasing the volume of molten metal, minimizing temperature distributions inside the reactor due to the high heat capacity of gallium. In addition, the catalytic activity of gallium can also play a role although it needs further validation. Phase segregation of carbon black from hydrogen was also achieved, validating the proof-of-concept. The techno-economic assessment showed that the variable operating costs dominate over the capital investment, being the acquisition costs of natural gas and gallium the highest. The sensitivity analyses highlighted that Cases 1 (partial burnt of carbon) and 4 (use of electricity) are highly competitive alternatives with the benchmark for different scenarios, proving their flexibility. An acute increase in the electricity costs could make Case 4 unfeasible, although current trends suggest cheaper electricity in the future. Considering high carbon taxes, as consequence of stricter environmental policies, the best TDNG configurations are thus Case 1 with capture and Case 4. The replacement of natural gas for renewable sources seems promising. For instance, the usage of biomass-based sources has been experimentally demonstrated and therefore a window for deeper research is opened. Furthermore, the produced carbon at industrial scale can be stored in perpetuity as carbon source, in case its demand is lower than its production. However, a new economic evaluation will be needed in this case to elucidate whether the technology is still profitable. The use of cheaper metals (e.g. Bi, Al) is also interesting to compare with the obtained results for gallium, and tin from literature. Nickel powder might be placed inside the molten metal bath in a slurry bubble column configuration to improve conversion at lower temperatures. For effective carbon separation, the use of molten salts is being tested in the field. Molten salts are inexpensive; thus it is worth to keep making efforts on this direction.

Declaration of competing interest

The authors declare that they have no known competing financial interests or personal relationships that could have appeared to influence the work reported in this paper.

Appendix A. Supplementary data

Supplementary data to this article can be found online at https://doi.org/10.1016/j.ijhydene.2020.11.079.

REFERENCES

[1] Berkeley Earth. October 2019 temperature. Update. 2019. http://berkeleyearth.org/october-2019-temperature-update-new/.

[2] Laboratories ESR. Global monitoring division at Mauna Loa. 2020. https://www.esrl.noaa.gov/gmd/ccgg/trends/mlo.html.

[3] Ashik UPM, Wan Daud WMA, Abbas HF. Production of greenhouse gas free hydrogen by thermocatalytic decomposition of methane - a review. Renew Sustain Energy Rev 2015;44:221–56. https://doi.org/10.1016/j.rser.2014.12.025.

[4] Parkinson B, Matthews JW, McConnaughy TB, Upham DC, McFarland EW. Techno-economic analysis of methane pyrolysis in molten metals: decarbonizing natural gas. Chem Eng Technol 2017;40:1022–30. https://doi.org/10.1002/ceat.201600414.

[5] Turner JA. Sustainable hydrogen production. Science 2004;305:972–5. https://doi.org/10.1007/978-3-319-41616-8 (80-).

[6] Ni M, Leung DYC, Leung MKH, Sumathy K. An overview of hydrogen production from biomass. Fuel Process Technol 2006;87:461–72. https://doi.org/10.1016/j.fuproc.2005.11.003.

[7] Medrano JA, Spallina V, Annaland MVS, Gallucci F. Thermodynamic analysis of a membrane-assisted chemical looping reforming reactor concept for combined H2 production and CO2 capture. Int J Hydrogen Energy 2013;39:4725–38. https://doi.org/10.1016/j.ijhydene.2013.11.126.

[8] Medrano JA, Potdar I, Melendez J, Spallina V, Pacheco-tanaka DA. The membrane-assisted chemical looping reforming concept for efficient H2 production with inherent CO2 capture : experimental demonstration and model validation. Appl Energy 2018;215:75–86. https://doi.org/10.1016/j.apenergy.2018.01.087.

[9] Wassie SA, Medrano JA, Zaabout A, Cloete S, Melendez J, Pacheco DA, et al. Hydrogen production with integrated CO2 capture in a membrane assisted gas switching reforming reactor: proof-of-Concept. Int J Hydrogen Energy 2018;43:6177–90. https://doi.org/10.1016/j.ijhydene.2018.02.040.

[10] Serban M, Lewis MA, Marshall CL, Doctor RD. Hydrogen production by direct contact pyrolysis of natural gas. Energy Fuels 2003;17:705–13. https://doi.org/10.1021/ef020271q.

[11] Abánades A, Ruíz E, Ferruelo EM, Hernández F, Martínez-Val JM, Cabanillas A, et al. Experimental analysis of direct thermal methane cracking. Int J Hydrogen Energy 2011;36:12877–86.

[12] Muradov NZ, Veziroğlu TN. "Green" path from fossil-based to hydrogen economy: an overview of carbon-neutral technologies. Int J Hydrogen Energy 2008;33:6804–39. https://doi.org/10.1016/j.ijhydene.2008.08.054.

[13] Muradov N, Smith F, T-Raissi A. Catalytic activity of carbons for methane decomposition reaction. Catal Today 2005;102–103:225–33. https://doi.org/10.1016/j.cattod.2005.02.018.

[14] Serrano DP, Botas JA, Guil-Lopez R. H2production from methane pyrolysis over commercial carbon catalysts: kinetic and deactivation study. Int J Hydrogen Energy 2009;34:4488–94. https://doi.org/10.1016/j.ijhydene.2008.07.079.

[15] Rodríguez-Reinoso F, Sepúlveda-Escribano A. Porous carbons in adsorption and catalysis. Handb Surfaces Interfaces Mater 2001;5:309–55. https://doi.org/10.1016/b978-012513910-6/50066-9.

[16] Wang M-J, Gray CA, Reznek SA, Mahmud K, Kutsovsky Y, Corporation C. Carbon black. Kirk-Othmer Encycl Chem Technol 2005;4.

[17] Keipi T, Tolvanen KES, Tolvanen H, Konttinen J. Thermo-catalytic decomposition of methane: the effect of reaction parameters on process design and the utilization possibilities of the produced carbon. Energy Convers Manag

2016;126:923–34. https://doi.org/10.1016/j.enconman.2016.08.060.
[18] Agency IE. Global trends and outlook for hydrogen. 2017.
[19] Agency IE. The future of hydrogen. Seizing today's opportunities. 2019.
[20] Weger L, Abánades A, Butler T. Methane cracking as a bridge technology to the hydrogen economy. Int J Hydrogen Energy 2017;42:720–31. https://doi.org/10.1016/j.ijhydene.2016.11.029.
[21] D. Tyrer, Production of hydrogen, United States Patent Office US1803221A. 1931:5–7.
[22] Steinberg M. Fossil fuel decarbonization technology for mitigating global warming. Int J Hydrogen Energy 1999;24:771–7. https://doi.org/10.1016/S0360-3199(98)00128-1.
[23] Wang K, Li WS, Zhou XP. Hydrogen generation by direct decomposition of hydrocarbons over molten magnesium. J Mol Catal A Chem 2008;283:153–7. https://doi.org/10.1016/j.molcata.2007.12.018.
[24] Vignes A. Extractive metallurgy 3: processing operations and routes. Hoboken, NJ: John Wiley & Sons, Ltd.; 2011.
[25] Duby PF. Metallurgy, Extractive. In: Kirk-Othmer Encyclopedia of Chemical Technology; 2005. https://doi.org/10.1002/0471238961.0524201804210225.a01.pub2.
[26] Esrafilzadeh D, Zavabeti A, Jalili R, Atkin P, Choi J, Carey BJ, et al. Room temperature CO2 reduction to solid carbon species on liquid metals featuring atomically thin ceria interfaces. Nat Commun 2019. https://doi.org/10.1038/s41467-019-08824-8.
[27] Upham DC, Agarwal V, Khechfe A, Snodgrass ZR, Gordon MJ, Metiu H, et al. Catalytic molten metals for the direct conversion of methane to hydrogen and separable carbon. Science 2017;358:917–21. https://doi.org/10.1126/science.aao5023 (80-).
[28] Kang D, Rahimi N, Gordon MJ, Metiu H, Mcfarland EW. Catalytic methane pyrolysis in molten MnCl2 -KCl. Appl Catal B Environ 2019;254:659–66. https://doi.org/10.1016/j.apcatb.2019.05.026.
[29] Kang D, Palmer C, Mannini D, Rahimi N, Gordon MJ, Metiu H, et al. Catalytic methane pyrolysis in molten alkali chloride salts containing iron. ACS Catal 2020;10:7032–42. https://doi.org/10.1021/acscatal.0c01262.
[30] Rahimi N, Kang D, Gelinas J, Menon A, Gordon MJ, Metiu H, et al. Solid carbon production and recovery from high temperature methane pyrolysis in bubble columns containing molten metals and molten salts. Carbon N Y 2019;151:181–91. https://doi.org/10.1016/j.carbon.2019.05.041.
[31] Schultz I, Agar DW. Decarbonisation of fossil energy via methane pyrolysis using two reactor concepts: fluid wall flow reactor and molten metal capillary reactor. Int J Hydrogen Energy 2015;40:11422–7. https://doi.org/10.1016/j.ijhydene.2015.03.126.
[32] Plevan M, Geißler T, Abánades A, Mehravaran K, Rathnam RK, Rubbia C, et al. Thermal cracking of methane in a liquid metal bubble column reactor: experiments and kinetic analysis. Int J Hydrogen Energy 2015;40:8020–33. https://doi.org/10.1016/j.ijhydene.2015.04.062.
[33] Geißler T, Plevan M, Abánades A, Heinzel A, Mehravaran K, Rathnam RK, et al. Experimental investigation and thermo-chemical modeling of methane pyrolysis in a liquid metal bubble column reactor with a packed bed. Int J Hydrogen Energy 2015;40:14134–46. https://doi.org/10.1016/j.ijhydene.2015.08.102.
[34] Geißler T, Abánades A, Heinzel A, Mehravaran K, Müller G, Rathnam RK, et al. Hydrogen production via methane pyrolysis in a liquid metal bubble column reactor with a packed bed. Chem Eng J 2016;299:192–200. https://doi.org/10.1016/j.cej.2016.04.066.
[35] Britton SC. Tin and tin alloys. In: Kirk-othmer encyclopedia of chemical technology, vol. 1. John Wiley & Sons, Ltd.; 2013. https://doi.org/10.1016/B978-0-08-052351-4.50048-0.
[36] Andreini RJ, Foster JS, Callen RW. Characterization of gas bubbles injected into molten metals under laminar flow conditions. Metall Trans B 1977;8:625–31. https://doi.org/10.1007/BF02658632.
[37] Heinzel A, Müller AWG. Corrosion behavior of austenitic steel AISI 316L in liquid tin in the temperature range between 280 and 700 ° C. Mater Corros 2017;1–7. https://doi.org/10.1002/maco.201609211.
[38] Spells KE. The determination of the viscosity of liquid gallium over an extended nrange of temperature. Proc Phys Soc 1936;48:299–311. https://doi.org/10.1088/0959-5309/48/2/308.
[39] Mazayev SN, Prokofiev YG. Hydrogen inventory in gallium. J Nucl Mater 1994;212–215. https://doi.org/10.1016/0022-3115(94)91077-4. 1497–8.
[40] Durinck D, Engström F, Arnout S, Heulens J, Tom P, Björkman B, et al. Resources , Conservation and Recycling Hot stage processing of metallurgical slags 2008;52:1121–31. https://doi.org/10.1016/j.resconrec.2008.07.001.
[41] Abánades A, Rubbia C, Salmieri D. Technological challenges for industrial development of hydrogen production based on methane cracking. Energy 2012;46:359–63. https://doi.org/10.1016/j.energy.2012.08.015.
[42] Fernandez ES, Goetheer ELV, Manzolini G, Macchi E, Rezvani S, Vlugt TJH. Thermodynamic assessment of amine based CO2 capture technologies in power plants based on European Benchmarking Task Force methodology. Fuel 2014;129:318–29. https://doi.org/10.1016/j.fuel.2014.03.042.
[43] Manzolini G, Fernandez ES, Rezvani S, Macchi E, Goetheer ELV, Vlugt TJH. Economic assessment of novel amine based CO 2 capture technologies integrated in power plants based on European Benchmarking Task Force methodology. Appl Energy 2015;138:546–58. https://doi.org/10.1016/j.apenergy.2014.04.066.
[44] Agarwal DC, Brill U, Wilson J. Combatting high temperature corrosion with alloy 602 CA (UNS N06025) in various environments and industries. Corrosion 2002:1–14.
[45] VDM T. Nicrofer 6025 HT - alloy 602CA.pdf. 2002.
[46] Wilson J, Agarwal DC. Case histories on successful applications for alloy 602 CA, UNS N06025 in high temperature environments. Corrosion 2005:1–14.
[47] Taddeo M. Assessing the effect a refractory insulation lining has on EAF energy consumption. 2014.
[48] Perry RH, Green DW. Perry's chemical engineers' handbook. 2008.
[49] International H. HAYNES ® 556 ® alloy. 2020.
[50] Science ST. Products & solutions - cooling. 2019. https://www.solexthermal.com/our-technology/cooling.
[51] Sutherland N, Nix A. Innovative cooling solution for biosolids. 2015.
[52] Spallina V, Pandolfo D, Battistella A, Romano MC, Van Sint Annaland M, Gallucci F. Techno-economic assessment of membrane assisted fluidized bed reactors for pure H2 production with CO2 capture. Energy Convers Manag 2016. https://doi.org/10.1016/j.enconman.2016.04.073.

[53] CaESAR. European best practice guidelines for assessment of CO2 capture technologies. 2011. p. 1–112.
[54] Martínez I, Romano MC, Chiesa P, Grasa G, Murillo R. Hydrogen production through sorption enhanced steam reforming of natural gas: thermodynamic plant assessment. Int J Hydrogen Energy 2013;38:15180–99. https://doi.org/10.1016/j.ijhydene.2013.09.062.
[55] Spallina V, Pandolfo D, Battistella A, Romano MC, Annaland MVS, Gallucci F. Techno-economic assessment of membrane assisted fluidized bed reactors for pure H 2 production with CO 2 capture. Energy Convers Manag 2016;120:257–73. https://doi.org/10.1016/j.enconman.2016.04.073.
[56] Energy USD of. Cost estimation methodology for NETL assessments of power plant performance. 2011.
[57] Manzolini G, Macchi E, Gazzani M. CO2 capture in natural gas combined cycle with SEWGS. Part B: economic assessment. Int J Greenh Gas Control 2013;12:502–9. https://doi.org/10.1016/j.ijggc.2012.06.021.
[58] Williams RJ. Six-tenths factor Aids in approximating costs. Chem Eng 1947;54:124–5.
[59] Manzolini G, di Milano P, Dijkstra J, Macchi E. Technical economic evaluation of a system for electricity production with CO2 capture using a membrane reformer with permeate side combustion. 2006. p. 1–11.
[60] Almeland SK, Meland K, Edvardsen D. Process design and economical assessment of a methanol plant. NTU; 2009.
[61] Pandolfo D. Techno-economic analysis of innovative systems of hydrogen production from natural gas with membrane reactors and low CO2 emissions. 2014. https://doi.org/10.1001/jama.2014.2634.
[62] Nexant. Equipment design and cost estimation for small modular biomass systems, synthesis gas cleanup, and oxygen separation equipment task 9 : mixed alcohols from syngas — state of technology. 2006.
[63] Kreutz T, Williams R, Consonni S, Chiesa P. Co-production of hydrogen, electricity and CO2 from coal with commercially ready technology. Part B: economic analysis. Int J Hydrogen Energy 2005;30:769–84. https://doi.org/10.1016/j.jasrep.2018.09.011.
[64] Sjostrom S, Denney J, Morris W. Optimizing the costs of solid sorbent - based CO2 capture process. Through heat integration. 2016.
[65] Birk Hill V. Exploring the benefits of alumina-forming alloys for furnace application. Ind Heat 2016.
[66] Ulrich G, Vasudevan PT. Chapter 4. Short-cut equipment design. Chem Eng Process Des Econ A Pract Guid 2004.
[67] Walas SM. Chapter 20: cost of individual equipment. Chem Process Equip Sel Des 1985:1–8.
[68] Campanari S, Chiesa P, Manzolini G, Bedogni S. Economic analysis of CO2capture from natural gas combined cycles using Molten Carbonate Fuel Cells. Appl Energy 2014;130:562–73. https://doi.org/10.1016/j.apenergy.2014.04.011.
[69] Level D. DECARBit Project full title: enabling advanced pre-combustion capture techniques and plants Collaborative large-scale integrating project European best practice guidelines for assessment of CO 2 capture technologies. 2011.
[70] MB F. Metal bulletin - daily. 9 April 2020.
[71] Administration UEI. Quarterly coal report april - june. 2018.
[72] Bokobza L, Bruneel J-L, Couzi M. Raman spectra of carbon-based materials (from graphite to carbon black) and of some silicone composites. C 2015;1:77–94. https://doi.org/10.3390/c1010077.
[73] Wall M. The Raman spectroscopy of graphene and the determination of layer thickness. Thermo Sci 2011;5.
[74] Dannenberg EM, Paquin L, Gwinnell H. Carbon Black. In: Kirk-Othmer Encyclopedia of Chemical Technology; 2000. https://doi.org/10.1002/0471238961.0301180204011414.a01.
[75] Keipi T, Hankalin V, Nummelin J, Raiko R. Techno-economic analysis of four concepts for thermal decomposition of methane: reduction of CO2 emissions in natural gas combustion. Energy Convers Manag 2016;110:1–12. https://doi.org/10.1016/j.enconman.2015.11.057.
[76] Knoema. Natural gas prices forecast: long term 2018 to 2030. Data and charts. 2019.